

Benchmarking neutral atom-based quantum processors at scale

Andrea B. Rava,^{1, 2, *} Kristel Michielsen,^{1, 3} and J. A. Montañez-Barrera^{1, †}

¹*Jülich Supercomputing Centre, Forschungszentrum Jülich, D-52425 Jülich, Germany*

²*RWTH Aachen University, 52056 Aachen, Germany*

³*Department of Computer Science, University of Cologne, 50931 Cologne, Germany*

In recent years, neutral atom-based quantum computation has been established as a competing alternative for the realization of fault-tolerant quantum computation. However, as with other quantum technologies, various sources of noise limit their performance. With processors continuing to scale up, new techniques are needed to characterize and compare them in order to track their progress. In this work, we present two systematic benchmarks that evaluate these quantum processors at scale. We use the quantum adiabatic algorithm (QAA) and the quantum approximate optimization algorithm (QAOA) to solve maximal independent set (MIS) instances of random unit-disk graphs. These benchmarks are scalable, relying not on prior knowledge of the system's evolution but on the quality of the MIS solutions obtained. We benchmark `quera_aquila` and `pasqal_fresnel` on problem sizes up to 102 and 85 qubits, respectively. Overall, `quera_aquila` performs better on QAOA and QAA instances. Finally, we generate MIS instances of up to 1000 qubits, providing scalable benchmarks for evaluating future, larger processors as they become available.

Keywords: Quantum Benchmarking, Aquila, Fresnel, neutral-atoms, Quantum Adiabatic Algorithm.

I. INTRODUCTION

Neutral atoms have rapidly emerged as one of the leading platforms for quantum computation and simulation, offering a unique combination of scalability, reconfigurability, and interaction control [1–5]. In these systems, individual atoms are trapped in optical tweezers or lattices and manipulated using laser light, while interactions are mediated through Rydberg excitations or spin-exchange mechanisms. This platform supports both analog and digital (gate-based) paradigms of quantum computation. In the analog mode, the dynamics of the system directly emulate the time evolution of a target Hamiltonian, making neutral atoms particularly suited for solving combinatorial optimization problems, quantum many-body dynamics, and quantum phase transitions [6–10]. In parallel, advances in coherent control, qubit initialization, and high-fidelity Rydberg-mediated entangling gates have also enabled gate-based neutral-atom quantum computing [11] with the demonstration of fault-tolerant elements [12, 13].

Several commercial and academic efforts, including QuEra Computing [14], Pasqal [15], Atom Computing [16], and Infleqtion [17], are now deploying large-scale neutral-atom processors featuring hundreds of atoms, with the prospect of scaling to thousands in the near term [18, 19]. The analog computing mode of these devices, often framed as programmable Rydberg simulators, allows for flexible encoding of the Maximum Independent Set (MIS) via effective Ising Hamiltonians.

As quantum processors continue to grow in complexity and scale, the demand for systematic benchmarking

protocols has become increasingly important. Benchmarking in quantum computing generally serves two complementary purposes: (i) to quantify the performance and noise characteristics of a given hardware platform, and (ii) to provide a fair, architecture-independent means of comparison between devices. Traditional approaches, such as randomized benchmarking (RB) [20], cross-entropy benchmarking (XEB) [21], and gate-set tomography [22], focus on gate fidelities and control errors, providing microscopic performance measures for gate-based architectures [23, 24]. However, for analog neutral-atom processors, benchmarking must go beyond individual gate errors and instead evaluate the algorithmic quality of analog evolution under realistic many-body Hamiltonians.

Recent works have started to address this challenge by using problem-based or dynamical benchmarks, for instance, measuring the success probability of adiabatic protocols or the fidelity of analog quantum simulations of known spin models [25, 26]. However, there is a need for a unified framework for comparing the analog performance of large-scale devices.

In this work, we introduce a scalable benchmarking methodology that evaluates analog neutral-atom quantum processors through the performance of the QAA [27] and the QAOA [28] to solve MIS instances of random unit-disk graphs. Our approach measures how effectively the analog dynamics of the system produce high-quality solutions to well-defined computational tasks. We apply this benchmark to QuEra's Aquila [29] and Pasqal's Fresnel [30], solving MIS problems up to 102 qubits and 85 qubits, respectively. We further generate benchmark instances for up to 1,000 qubits, providing a scalable testbed for assessing future devices as they grow in size and complexity.

Figure 1 summarizes this approach. In Fig. 1(a), the arrangement of the atoms and the considered MIS prob-

* a.rava@fz-juelich.de

† j.montanez-barrera@fz-juelich.de

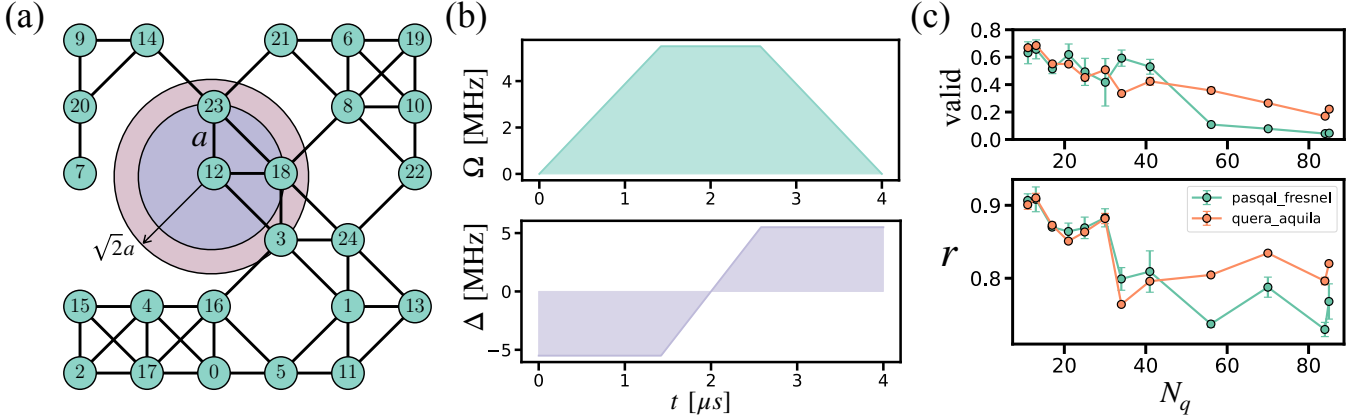


FIG. 1. Benchmarking of neutral atom quantum devices. (a) Arrangement of the neutral atoms for the solution of a 25-qubit instance. a is the minimum distance between atoms, and $\sqrt{2}a$ is the distance where a Rydberg interaction is considered strongly enough to encode an edge of the MIS. (b) QAA protocol for a $t = 4\ \mu\text{s}$. (c) Valid solutions (up) and approximation ratio (down), r , for problem sizes between 11 and 85 qubits for *quera_aquila* and *pasqal_fresnel*. Error bars represent the standard deviation for 3 experiments of 500 samples each.

lem is encoded. (b) The QAA schedule, if implemented correctly and depending on the noise level, should yield high-quality solutions to the MIS problem. (c) Experimental results on the two quantum processing units (QPUs) tested in terms of the proportion of valid solutions found, the approximation ratio, r , versus the number of qubits N_q .

The paper is organized as follows. Section II provides a description of MIS, QAA, QAOA, and the experimental setup. In Sec. III, the results of QAA and QAOA on real QPUs are presented. Finally, Sec. IV provides some conclusions.

II. METHODS

A. Maximal independent set problem

In graph theory, an independent set is a collection of vertices in a graph such that no two are connected by an edge. The task of finding the Maximum Independent Set (MIS), the largest such subset, is a well-known NP-hard problem [31], meaning that no efficient (i.e., polynomial-time) algorithm is known to solve it for arbitrary graphs. For the MIS problem on a graph with N_q vertices and edge set E , the cost function is

$$C(\vec{x}) = \sum_{i=1}^{N_q} x_i - \lambda_0 \sum_{(i,j) \in E} x_i x_j, \quad (1)$$

where λ_0 is a penalty coefficient to avoid solutions that do not fulfill the MIS constraints.

The quantity used to evaluate a solver ability to find good solutions to this problem is known as the approxi-

mation ratio, r . It is defined as

$$r = \frac{\sum_i^n C(\vec{x}_i) - C_{\text{worst}}}{C_{\text{opt}} - C_{\text{worst}}}, \quad (2)$$

where \vec{x}_i are the n solutions obtained with the solver, C_{opt} and C_{worst} are the optimal and worst possible values of $C(\vec{x})$ defined in Eq. 1. This ratio lies in the interval $0 \leq r \leq 1$, where higher values indicate better solutions on average. In our case, we only consider the valid solutions found and therefore, $C_{\text{worst}} = 0$.

Another useful performance metric is the success probability, $\text{probability}(x^*)$, defined as the fraction of measurement outcomes that correspond to the optimal solutions $\{x_{i^*}\}$.

The quantum version of the objective function is defined in a 2_q^N -dimensional Hilbert space with computational basis states $|z\rangle \in \{|0\rangle, |1\rangle\}^{\otimes N_q}$. The classical cost function is converted to a diagonal Hamiltonian \hat{H}^C by mapping each bit x_i to the occupation operator $\hat{n} = (1 + \hat{\sigma}_i^z)/2$,

$$\hat{H}^C = \sum_i^{N_q} \left(w_i \hat{n}_i + \sum_{j < i} l_{ij} \hat{n}_i \hat{n}_j \right), \quad (3)$$

where w_i and l_{ij} are real-valued weights.

The MIS constraints map naturally onto the Rydberg blockade phenomenon in neutral-atom quantum computing. Specifically, the Rydberg blockade prevents two nearby atoms from being simultaneously excited to a Rydberg state $|r\rangle$, mirroring the MIS condition that connected vertices cannot both be included in the independent set [32]. The Rydberg Hamiltonian that describes this phenomenon is given by

$$\hat{H}_{\text{Ryd}} = \sum_i^{N_q} \left[\frac{\Omega(t)\hbar}{2} \hat{\sigma}_i^x - \Delta(t)\hbar \hat{n}_i + \sum_{j < i} V_{ij} \hat{n}_i \hat{n}_j \right], \quad (4)$$

where $V_{ij} = C_6/R_{ij}^6$ is the interaction between atoms i and j at distance R_{ij} , and C_6 is the Rydberg interaction constant.

This correspondence allows us to encode the MIS problem directly into the ground state of the Rydberg Hamiltonian. For certain geometric graphs, particularly unit disk graphs (UDGs), where vertices represent points in the plane and edges connect pairs within a fixed distance, this encoding can be achieved without any overhead in the number of qubits, using each atom to represent a single graph vertex [8].

In this work, we use Diagonal-connected Unit-disk Grid Graphs (DUGGs), such as the one in Fig. 1(a). Despite their constrained and regular structure, finding the MIS for such graphs remains NP-hard [8] and a non-trivial task on neutral atom-based quantum processing units (QPUs).

We arrange the atoms on a square grid such that both nearest neighbors (horizontal and vertical) and next-nearest neighbors (diagonal) fall within the unit disk interaction range. As a result, in the associated graph, edges connect both adjacent and diagonally neighboring vertices. To generate a variety of graph instances, we apply a random dropout process to square grids of varying sizes, controlling the density by adjusting the probability that each site is occupied by an atom.

B. QAA algorithm

The core idea of the QAA (also known as Quantum Annealing) is to exploit the adiabatic theorem: if a quantum system starts in the ground state of an initial Hamiltonian and evolves sufficiently slowly, it will remain in the instantaneous ground state of the time-dependent Hamiltonian throughout the evolution [33]. By designing the final Hamiltonian so that its ground state encodes the solution to a desired optimization problem, the system ideally ends up in that solution state at the end of the evolution.

For Rydberg-atom-based quantum devices, this adiabatic evolution can be naturally implemented using the tunable Rydberg Hamiltonian parameters. Since the initial state of the device is prepared with all atoms in their electronic ground state $|0\rangle$, we choose the initial Hamiltonian such that this state is indeed its ground state. This is readily achieved by setting the initial detuning to a large negative value, $\Delta(t=0) = \Delta_{\text{in}} < 0$, and keeping the Rabi driving field off, i.e., $\Omega(t=0) = 0$. In this configuration, the ground state corresponds trivially to all qubits in $|0\rangle$.

The adiabatic evolution proceeds in three main stages (See Fig. 1(b)):

- **Ramp-up of the driving field:** Over an initial time interval t_{rise} , the Rabi frequency $\Omega(t)$ is increased linearly from 0 to a chosen maximum value Ω_{max} , while keeping the detuning Δ fixed at Δ_{in} .

This activates coherent transitions that enable superpositions and tunneling between different classical configurations.

- **Sweeping the detuning:** During a period t_{sweep} , the driving field is held constant at Ω_{max} , while the detuning $\Delta(t)$ is linearly swept from the initial negative value Δ_{in} to a final positive value Δ_{fin} . This sweep biases the Hamiltonian towards the configurations that solve the MIS.
- **Ramp-down of the driving field:** In the final interval t_{fall} , the detuning $\Delta(t)$ is kept fixed at Δ_{fin} , while the driving field $\Omega(t)$ is linearly ramped back down to zero. This effectively suppresses further quantum fluctuations.

C. QAOA algorithm

In general, an optimization problem can be formulated as minimizing a cost function $C(\vec{x})$ that encodes the problem's constraints and depends on a binary variable vector $\vec{x} = (x_0, x_1, \dots, x_{N_q})^T$, with $x_i \in \{0, 1\}$. The goal is to find the bitstring \vec{x}^* that minimizes $C(\vec{x})$.

QAOA prepares a quantum state with high probability of yielding a near-optimal bitstring \vec{x} by optimizing over variational parameters. The procedure consists of:

1. Initial state: Prepare the uniform superposition $|s\rangle = |+\rangle^{\otimes N_q}$.
2. Variational evolution: Apply p layers of alternating unitaries generated by \hat{H}^C and a mixing Hamiltonian \hat{H}^B , parameterized by $(\vec{\gamma}, \vec{\beta})$

$$|\vec{\gamma}, \vec{\beta}\rangle = \hat{U}_p^M \hat{U}_p^C \cdots \hat{U}_1^B \hat{U}_1^C |s\rangle, \quad (5)$$

where $\hat{U}_k^C = e^{-i\gamma_k \hat{H}^C}$ and $\hat{U}_k^M = e^{-i\beta_k \hat{H}^M}$ and the mixing Hamiltonian is $\hat{H}^M = \sum_{j=1}^{N_q} \hat{\sigma}_j^x$.

3. Measurement: Estimate the expectation value of the cost Hamiltonian

$$F_p(\vec{\gamma}, \vec{\beta}) = \langle \vec{\gamma}, \vec{\beta} | \hat{H}^C | \vec{\gamma}, \vec{\beta} \rangle, \quad (6)$$

using n_{shots} samples:

$$F_p = \frac{\sum_{i=1}^{n_{\text{shots}}} w_i C(\vec{x}_i)}{n_{\text{shots}}}, \quad (7)$$

where w_i counts occurrences of bitstring \vec{x}_i .

4. Classical optimization: perform steps 1–3 in an optimization loop to minimize F_p over $(\vec{\gamma}, \vec{\beta})$. In this work, we used the Nelder-Mead simplex method [34] as classical optimizer.

The correspondence between QAOA cost Hamiltonian, Eq.3, \hat{H}^M , and the Rydberg Hamiltonian, Eq. 4 can be described as follows. The \hat{n}_i and $\sum_{j < i} V_{ij} \hat{n}_i \hat{n}_j$ correspond to the cost function, while $\hat{\sigma}_i^x$ acts as a mixing term. The QAOA parameters γ_k and β_k correspond to different values Δ_k and Ω_k , respectively.

However, implementing QAOA using neutral atoms differs in three key ways. First, the initial state is the all-down state $|0\rangle^{\otimes N_q}$. Second, the interaction term is always active, making it impossible to isolate the mixing Hamiltonian during evolution. Finally, in our implementation, the $\Omega(t)$ and $\Delta(t)$ pulses act simultaneously, rather than in the alternating layers characteristic of QAOA.

D. Transfer learning on QAOA

Transfer learning (TL) refers to reusing pre-optimized QAOA parameters from one problem instance on different instances [35], thereby reducing the need for costly classical optimization for each new problem. This means applying pre-trained parameters $\vec{\gamma} = (\gamma_1, \gamma_2, \dots, \gamma_p)$ and $\vec{\beta} = (\beta_1, \beta_2, \dots, \beta_p)$ to problem instances not used during the original optimization. The approach involves first optimizing the parameters for a specific instance, then evaluating their performance on other instances.

We optimized QAOA parameters for $p = 10$ and total evolution time $t_{\text{tot}} = 2 \mu\text{s}$ simultaneously on 12 randomly generated DUGGs with system sizes between 10 and 12 qubits, using the JUelich Quantum Annealing Simulator (JUQAS), which solves the Schrödinger equation using the Suzuki-Trotter product-formula algorithm [36–40].

For the emulations, the starting point was the annealing schedule of Fig. 1(b), and the average over the 12 problems is taken to ensure that the parameters obtained work for different problems. The optimized parameter schedules is shown in Fig. 2.

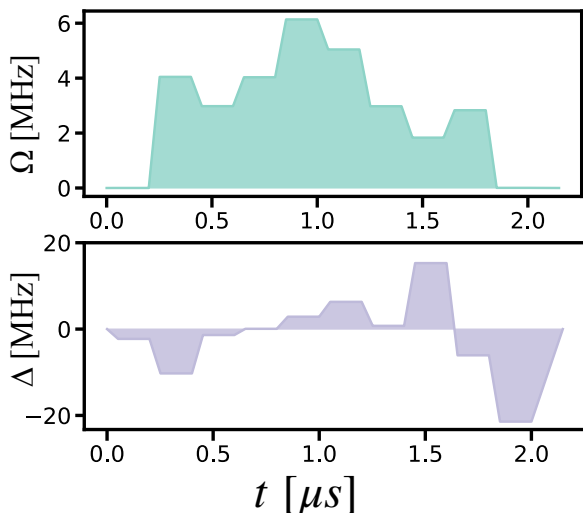


FIG. 2. Optimized schedule for the QAOA protocol.

	Fresnel	Aquila
C_6	865723 MHz	5420441 MHz
max num. atoms	100	256
a_{min}	$5 \mu\text{m}$	$4 \mu\text{m}$
t_{max}	$6 \mu\text{s}$	$4 \mu\text{s}$
Ω_{max}	$2 \times 2\pi \text{ MHz}$	$2.5 \times 2\pi \text{ MHz}$
$ \Delta _{\text{max}}$	$7.75 \times 2\pi \text{ MHz}$	$20 \times 2\pi \text{ MHz}$

TABLE I. Specifications of `quera_aquila` and `pasqal_fresnel`.

E. Experimental setup

The experiments are executed on two neutral atom QPUs, Fresnel from Pasqal, `pasqal_fresnel`, and Aquila from QuEra, `quera_aquila` [41]. Their main specifications are listed in Table I. For the experimental results, we took 500 samples for each problem size on three different days on each device for both the QAOA and QAA protocols.

For QAOA parameters optimization, we used an emulator with an interaction coefficient $C_6 = 865723 \text{ MHz}$, matching that of Fresnel. To apply the same schedule to Aquila, which has a different C_6 , we ensure consistent interaction strengths by using the condition

$$C_6^{\text{Fresnel}} / a_{\text{Fresnel}}^6 = C_6^{\text{Aquila}} / a_{\text{Aquila}}^6, \quad (8)$$

where a is the distance between adjacent atoms, and for `pasqal_fresnel` is used $a_{\text{Fresnel}} = 5 \mu\text{m}$ which corresponds to $a_{\text{Aquila}} = 6.79 \mu\text{m}$ for `quera_aquila`.

For the QAA, we employed the schedule structure defined in Section II B. We used fixed values for the driving field and detunings: $\Omega_{\text{max}} = 5.5 \text{ MHz}$, $\Delta_{\text{in}} = -5.5 \text{ MHz}$, and $\Delta_{\text{fin}} = 5.5 \text{ MHz}$. The total evolution time t_{tot} was varied across different experiments to investigate adiabaticity and solution quality. The ramp-up (t_{rise}) and ramp-down (t_{fall}) durations for $\Omega(t)$ were scaled accordingly with t_{tot} to maintain a symmetric profile. The detuning $\Delta(t)$ was linearly swept during a central interval t_{sweep} , as described in Section II B.

Measurement noise and atom loss are major challenges in analog quantum computing, and the two platforms address them differently. In `pasqal_fresnel`, only atoms that remain trapped are detected, so both Rydberg excitations and lost atoms appear as missing, creating ambiguity that must be modeled through SPAM parameters: η for preparation errors, ϵ for false positives, and ϵ' for false negatives. In contrast, `quera_aquila` provides detailed shot-level diagnostics, reporting whether readout errors occurred in each run. This enables post-selection to discard faulty bitstrings.

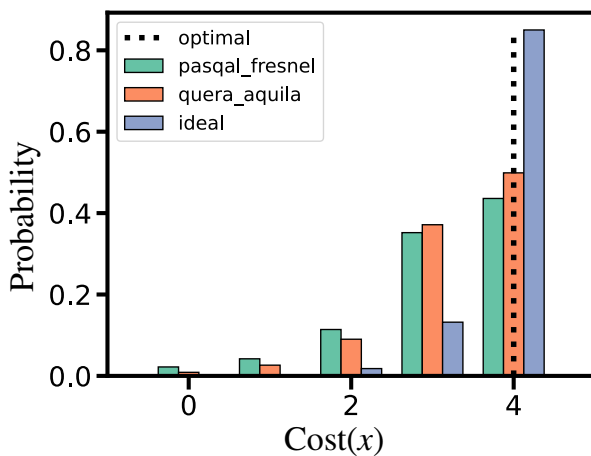


FIG. 3. Probability distribution of different solutions comparing `quera_aquila`, `pasql_fresnel`, and an ideal (noiseless) simulator for a problem with 13 qubits using QAA with $t = 4\mu\text{s}$.

III. RESULTS

Figure 3 shows the probability versus cost function of valid solutions for a 13-qubit MIS problem using `quera_aquila`, `pasql_fresnel`, and an ideal simulator. The optimal solution in this case involves 4 vertices and both QPUs can find it with large probability over the 500 samples taken, but still is below the ideal result. This is a consequence of noise, and the majority of the solutions of both solvers are still valid, but they differ in one or two from the optimal.

Extended results of solution quality versus number of qubits are given in Table II and Fig. 1(c) which summarizes the results for system sizes up to 85 qubits for the $4\mu\text{s}$ QAA schedule, using both the approximation ratio and the fraction of valid solutions as performance metrics. For problem sizes $N_q \leq 30$, the two QPUs exhibit comparable behaviour. Although `pasql_fresnel` shows slightly better performance at $N_q = 34$ and $N_q = 41$, the overall trend indicates that `quera_aquila` outperforms `pasql_fresnel`.

After a recent upgrade of `pasql_fresnel`, we were able to conduct experiments for $N_q > 41$. For these experiments, the quality of the solutions on `pasql_fresnel` drops to less than 11% for $N_q > 41$, which might indicate problems with the setup when operating the device at these scales.

Figure 4 compares QAOA and QAA performance for both QPUs. For the $2\mu\text{s}$ schedule, `quera_aquila` consistently outperforms `pasql_fresnel`. In particular, `pasql_fresnel` is less likely to find optimal solutions under QAOA protocol, an indication that implementing rapid variations of the driving fields might cause a degradation in the solution quality.

For QAOA, neither device finds the optimal solution for $N_q > 30$ qubits, which is a consequence of sam-

N_q	r		valid	
	Fresnel	Aquila	Fresnel	Aquila
11	0.9066	0.9008	0.632	0.669
13	0.9082	0.9101	0.657	0.685
17	0.8700	0.8726	0.515	0.551
21	0.8641	0.8509	0.619	0.550
25	0.8691	0.8634	0.493	0.452
30	0.8828	0.8819	0.417	0.508
34	0.7991	0.7641	0.593	0.335
41	0.8092	0.7959	0.530	0.424
56	0.7372	0.8045	0.109	0.357
70	0.7877	0.8344	0.078	0.265
84	0.7297	0.7962	0.043	0.170
85	0.7682	0.8201	0.046	0.221

TABLE II. QAA for $t = 4\mu\text{s}$ approximation ratio and valid solution fractions for `pasql_fresnel` and `quera_aquila`.

pling size, difficulty in implementing the algorithm on the QPUs, and the own performance of QAOA at $2\mu\text{s}$. Fig. 4(right) shows the QAA results at $N_q > 30$. For problem sizes up to 56 qubits, `pasql_fresnel` finds the optimal solution even at $2\mu\text{s}$ while `quera_aquila` finds it at least once in three experiments for up to $N_q = 85$.

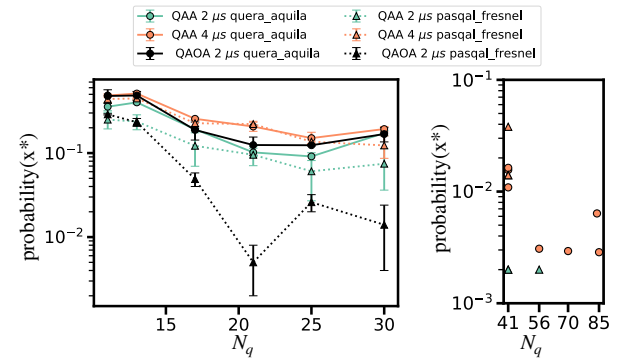


FIG. 4. Probability of success vs. number of qubits for QAOA and QAA on `quera_aquila` and `pasql_fresnel`. (left) $N_q \leq 30$ (right) $N_q > 30$.

Finally, Figure 5 shows the QAA best result obtained for each QPU at $t = 4\mu\text{s}$. We could not implement problems larger than $N_q > 85$ on `pasql_fresnel`, so there are no points above it. Up to 56 qubits, both QPUs find the optimal solution at least once. As the system size increases, the probability of finding the optimal solution gradually degrades, which is expected because the problems are more difficult to solve, and noise might impact the solution quality.

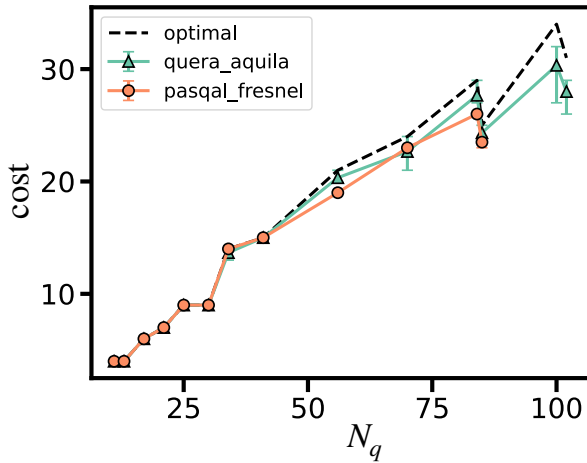


FIG. 5. Cost of the best solution found versus number of qubits for QAA and $t = 4\mu\text{s}$. The dashed line represents the optimal cost for each instance. The error bars represent the standard deviation over the 3 experiments.

IV. DISCUSSION AND CONCLUSIONS

In this work, we have presented two benchmarking strategies for neutral atom-based quantum computers that can be used for cross-platform evaluation, specifically to analyze a device's performances through QAA or QAOA results. The benchmarking strategy does not rely on previous knowledge of the ideal evolution of the system, but on the quality of the solutions obtained from the QPUs. We have tested the proposed method on `quera_aquila` and `pasqal_fresnel` with up to 102 qubits, and execution time between 2 and $4\mu\text{s}$.

The relationship between the atomic distances a and the interaction coefficients C_6 of the two devices Eq. (8) ensures equivalent interaction strengths and thus equivalent Hamiltonians, which enables the cross-platform benchmarking.

Overall, the ability of the QPUs to find valid and good-quality solutions degraded as the problem size increased. For example, for the 11-qubit problem, `pasqal_fresnel` gives 63.2% of valid solutions, while `quera_aquila` gives 66.9%, but for the 85-qubit problem, the valid solutions drop to 4.6% and 22.1%, respectively. In terms of quality of solutions, `quera_aquila` performs better than `pasqal_fresnel`, except for the $4\mu\text{s}$ QAA schedule at system sizes $N_q = 34, 41$, where `pasqal_fresnel` shows slightly better performance. However, the trend does not continue at larger problem sizes `pasqal_fresnel` again drops below that of `quera_aquila`. Across all tested conditions, QAOA does not systematically outperform QAA, although for identical evolution times, it performs better on `quera_aquila`. Nonetheless, QAOA remains valuable for benchmarking, as it provides insight into how each device handles non-uniform, fast-varying control schedules.

Finally, since the QAOA schedule used here was op-

timized via ideal emulations, an interesting direction for future work would be to explore whether further improvements can be achieved by optimizing the parameters in the presence of noise or by employing variational hybrid loops that combine classical optimization with quantum resources. Similarly, variational methods could also be applied to enhance QAA performance.

DATA AVAILABILITY

All problem instances are available at <https://jugit.fz-juelich.de/juniq/benchmark-suite/mis-udg>, and results analyzed in this study are available at <https://github.com/alejomonbar/Benchmarking-neutral-atom-QPUs>.

ACKNOWLEDGMENTS

J. A. Montanez-Barrera and A. B. Rava acknowledge support from the project Jülich UNified Infrastructure for Quantum computing (JUNIQ) that has received funding from the German Federal Ministry of Research, Technology, and Space (BMFTR) and the Ministry of Culture and Science of the State of North Rhine-Westphalia (MKW-NRW). A. B. Rava acknowledges support from the project HPCQS (101018180) of the European High-Performance Computing Joint Undertaking (EuroHPC JU). J. A. Montanez-Barrera acknowledges support from the project EPIQ funded by MKW-NRW. The authors gratefully acknowledge the Gauss Centre for Supercomputing e.V. (www.gauss-centre.eu) for funding this project by providing computing time on the GCS Supercomputer JUWELS Booster at Jülich Supercomputing Centre (JSC).

We acknowledge support from Amazon Web Services (AWS) through the provision of Amazon Braket credits used for quantum computing experiments on `quera_aquila`.

[1] A. Browaeys and T. Lahaye, Many-body physics with individually controlled rydberg atoms, *Nature Physics* **16**, 132 (2020).

[2] H. Bernien, S. Schwartz, A. Keesling, H. Levine, A. Omran, H. Pichler, S. Choi, A. S. Zibrov, M. Endres, M. Greiner, *et al.*, Probing many-body dynamics on a 51-atom quantum simulator, *Nature* **551**, 579 (2017).

[3] D. Bluvstein, A. Omran, H. Levine, A. Keesling, G. Semeghini, S. Ebadi, T. T. Wang, A. A. Michailidis, N. Maskara, W. W. Ho, *et al.*, Controlling quantum many-body dynamics in driven rydberg atom arrays, *Science* **371**, 1355 (2021).

[4] Y. Cheng and H. Zhai, Emergent $u(1)$ lattice gauge theory in rydberg atom arrays, *Nature Reviews Physics* **6**, 566 (2024).

[5] Q. Xu, J. P. B. Ataides, C. A. Pattison, N. Raveendran, D. Bluvstein, J. Wurtz, B. Vasic, M. D. Lukin, L. Jiang, and H. Zhou, Constant-overhead fault-tolerant quantum computation with reconfigurable atom arrays, *Nature Physics* **20**, 1084 (2024).

[6] M. Saffman, T. G. Walker, and K. Mølmer, Quantum information with rydberg atoms, *Rev. Mod. Phys.* **82**, 2313 (2010).

[7] A. Browaeys and T. Lahaye, Many-body physics with individually controlled rydberg atoms, *Nature Physics* **16**, 132–142 (2020).

[8] S. Ebadi, A. Keesling, M. Cain, T. T. Wang, H. Levine, D. Bluvstein, G. Semeghini, A. Omran, J.-G. Liu, R. Samajdar, X.-Z. Luo, B. Nash, X. Gao, B. Barak, E. Farhi, S. Sachdev, N. Gemelke, L. Zhou, S. Choi, H. Pichler, S.-T. Wang, M. Greiner, V. Vuletić, and M. D. Lukin, Quantum optimization of maximum independent set using rydberg atom arrays, *Science* **376**, 1209–1215 (2022).

[9] L. Bombieri, Z. Zeng, R. Tricarico, R. Lin, S. Notar Nicola, M. Cain, M. D. Lukin, and H. Pichler, Quantum adiabatic optimization with rydberg arrays: Localization phenomena and encoding strategies, *PRX Quantum* **6**, 10.1103/prxquantum.6.020306 (2025).

[10] M. J. A. Schuetz, R. Yalovetzky, R. S. Andrist, G. Salton, Y. Sun, R. Raymond, S. Chakrabarti, A. Acharya, R. Shaydulin, M. Pistoia, and H. G. Katzgraber, qredumis: A quantum-informed reduction algorithm for the maximum independent set problem (2025), arXiv:2503.12551 [quant-ph].

[11] N. Wagner, C. Poole, T. M. Graham, and M. Saffman, Benchmarking a neutral-atom quantum computer, *International Journal of Quantum Information* **22**, 10.1142/s0219749924500011 (2024).

[12] P. Sales Rodriguez, J. M. Robinson, P. N. Jepsen, Z. He, C. Duckering, C. Zhao, K.-H. Wu, J. Campo, K. Bagnall, M. Kwon, T. Karolyshyn, P. Weinberg, M. Cain, S. J. Evered, A. A. Geim, M. Kalinowski, S. H. Li, T. Manovitz, J. Amato-Grill, J. I. Basham, L. Bernstein, B. Braverman, A. Bylinskii, A. Choukri, R. J. DeAngelo, F. Fang, C. Fieweger, P. Frederick, D. Haines, M. Hamdan, J. Hammett, N. Hsu, M.-G. Hu, F. Huber, N. Jia, D. Kedar, M. Kornjača, F. Liu, J. Long, J. Lopatin, P. L. S. Lopes, X.-Z. Luo, T. Macrì, O. Marković, L. A. Martínez-Martínez, X. Meng, S. Ostermann, E. Ostroumov, D. Paquette, Z. Qiang, V. Shofman, A. Singh, M. Singh, N. Sinha, H. Thoreen, N. Wan, Y. Wang, D. Waxman-Lenz, T. Wong, J. Wurtz, A. Zhdanov, L. Zheng, M. Greiner, A. Keesling, N. Gemelke, V. Vuletić, T. Kitagawa, S.-T. Wang, D. Bluvstein, M. D. Lukin, A. Lukin, H. Zhou, and S. H. Cantú, Experimental demonstration of logical magic state distillation, *Nature* **645**, 620–625 (2025).

[13] H. Zhou, C. Zhao, M. Cain, D. Bluvstein, N. Maskara, C. Duckering, H.-Y. Hu, S.-T. Wang, A. Kubica, and M. D. Lukin, Low-overhead transversal fault tolerance for universal quantum computation, *Nature* **646**, 303–308 (2025).

[14] Quera computing inc., <https://www.quera.com/> (2025), accessed: 2025-11-05.

[15] Pasqal - quantum processing with neutral atoms, <https://www.pasqal.com/> (2025), accessed: 2025-11-05.

[16] Atom computing, inc., <https://atom-computing.com/quantum-computing-technology/> (2025), accessed: 2025-11-05.

[17] Infleqtion, <https://infleqtion.com/> (2025), accessed: 2025-11-05.

[18] L. Henriet, L. Beguin, A. Signoles, T. Lahaye, A. Browaeys, G.-O. Reymond, and C. Jurczak, Quantum computing with neutral atoms, *Quantum* **4**, 327 (2020).

[19] J. Wurtz, A. Bylinskii, B. Braverman, J. Amato-Grill, S. H. Cantu, F. Huber, A. Lukin, F. Liu, P. Weinberg, J. Long, S.-T. Wang, N. Gemelke, and A. Keesling, Aquila: Quera's 256-qubit neutral-atom quantum computer (2023), arXiv:2306.11727 [quant-ph].

[20] E. Knill, D. Leibfried, R. Reichle, J. Britton, R. B. Blakestad, J. D. Jost, C. Langer, R. Ozeri, S. Seidelin, and D. J. Wineland, Randomized benchmarking of quantum gates, *Physical Review A* **77**, 10.1103/physreva.77.012307 (2008).

[21] S. Boixo, S. V. Isakov, V. N. Smelyanskiy, R. Babbush, N. Ding, Z. Jiang, M. J. Bremner, J. M. Martinis, and H. Neven, Characterizing quantum supremacy in near-term devices, *Nature Physics* **14**, 595–600 (2018).

[22] E. Nielsen, J. K. Gamble, K. Rudinger, T. Scholten, K. Young, and R. Blume-Kohout, Gate set tomography, *Quantum* **5**, 557 (2021).

[23] R. Blume-Kohout, J. K. Gamble, E. Nielsen, J. Mizrahi, J. D. Sterk, and P. Maunz, Robust, self-consistent, closed-form tomography of quantum logic gates on a trapped ion qubit (2013), arXiv:1310.4492 [quant-ph].

[24] E. Magesan, J. M. Gambetta, and J. Emerson, Scalable and robust randomized benchmarking of quantum processes, *Phys. Rev. Lett.* **106**, 180504 (2011).

[25] S. Ebadi, T. T. Wang, H. Levine, A. Keesling, G. Semeghini, A. Omran, D. Bluvstein, R. Samajdar, H. Pichler, W. W. Ho, S. Choi, S. Sachdev, M. Greiner, V. Vuletić, and M. D. Lukin, Quantum phases of matter on a 256-atom programmable quantum simulator, *Nature* **595**, 227–232 (2021).

[26] D. Bluvstein, H. Levine, G. Semeghini, T. T. Wang, S. Ebadi, M. Kalinowski, A. Keesling, N. Maskara, H. Pichler, M. Greiner, V. Vuletić, and M. D. Lukin, A quantum processor based on coherent transport of entangled atom arrays, *Nature* **604**, 451–456 (2022).

[27] T. Keating, K. Goyal, Y.-Y. Jau, G. W. Biedermann, A. J. Landahl, and I. H. Deutsch, Adiabatic quantum

computation with rydberg-dressed atoms, *Physical Review A* **87**, 10.1103/physreva.87.052314 (2013).

[28] S. Tibaldi, L. Leclerc, D. Vodola, E. Tignone, and E. Ercolelli, Analog qaoa with bayesian optimisation on a neutral atom qpu (2025), arXiv:2501.16229 [quant-ph].

[29] J. Wurtz, A. Bylinskii, B. Braverman, J. Amato-Grill, S. H. Cantu, F. Huber, A. Lukin, F. Liu, P. Weinberg, J. Long, S.-T. Wang, N. Gemelke, and A. Keesling, Aquila: Quera's 256-qubit neutral-atom quantum computer (2023), arXiv:2306.11727 [quant-ph].

[30] Pasqal fresnel (2022), accessed: 2025-11-05.

[31] D. Hespe, S. Lamm, and C. Schorr, Targeted branching for the maximum independent set problem (2021), arXiv:2102.01540 [cs.DS].

[32] H. Pichler, S.-T. Wang, L. Zhou, S. Choi, and M. D. Lukin, Quantum optimization for maximum independent set using rydberg atom arrays (2018), arXiv:1808.10816 [quant-ph].

[33] B. Žunkovič, P. Torta, G. Pecci, G. Lami, and M. Collura, Variational ground-state quantum adiabatic theorem (2024), arXiv:2406.12392 [quant-ph].

[34] K. I. M. McKinnon, Convergence of the nelder-mead simplex method to a nonstationary point, *SIAM Journal on Optimization* **9**, 148 (1998), <https://doi.org/10.1137/S1052623496303482>.

[35] J. A. Montañez-Barrera, D. Willsch, and K. Michielsen, Transfer learning of optimal qaoa parameters in combinatorial optimization, *Quantum Information Processing* **24**, 10.1007/s11128-025-04743-4 (2025).

[36] M. Suzuki, Generalized Trotter's formula and systematic approximants of exponential operators and inner derivations with applications to many-body problems, *Commun. Math. Phys.* **51**, 83 (1976).

[37] M. Suzuki, Decomposition formulas of exponential operators and Lie exponentials with some applications to quantum mechanics and statistical physics, *J. Math. Phys.* **26**, 601 (1985).

[38] H. F. Trotter, On the product of semi-groups of operators, *Proc. Amer. Math. Soc.* **10**, 545 (1959).

[39] H. De Raedt, Product formula algorithms for solving the time dependent Schrödinger equation, *Comp. Phys. Rep.* **7**, 1 (1987).

[40] J. Huyghebaert and H. De Raedt, Product formula methods for time-dependent Schrödinger problems, *J. Phys. A: Math. Gen.* **23**, 5777 (1990).

[41] J. Wurtz, A. Bylinskii, B. Braverman, J. Amato-Grill, S. H. Cantu, F. Huber, A. Lukin, F. Liu, P. Weinberg, J. Long, S.-T. Wang, N. Gemelke, and A. Keesling, Aquila: Quera's 256-qubit neutral-atom quantum computer (2023), arXiv:2306.11727 [quant-ph].